From *Proceedings, BOSS-97: Behaviour of Offshore Structures*
Volume 2 (Hydrodynamics), ed. J.Vugts, Delft Univ, 1997, pp. 333–347.

Motions of a Spar Buoy in Random Seas: Comparing Predictions and Model Test Results

Alok K. Jha, P. R. de Jong, and Steven R. Winterstein

Civil Engineering Dept., Stanford University

Abstract

This study compares the analytically predicted motions of a floating spar buoy platform with the results of wave tank experiments. Results studied include extreme conditions in both the Gulf of Mexico and the North Sea. Base-case predictions combine nonlinear diffraction loads and a linear, multi-degree-of-freedom model of the spar stiffness and damping characteristics. Refined models add the effect of wave-drift damping, and of viscous forces as well. Consistent choices of damping and wave input are considered in some detail. These successive model refinements are generally found to improve agreement with the model test results.

Keywords

Nonlinear wave diffraction; offshore structures; random vibration; spar buoys, structural reliability; wave tank experiments.

Introduction

This study describes ongoing research into the statistical response behavior and reliability of a particular deep-water floating structure: a spar buoy. Typically, the spar buoy concept involves a deep-draft, large-diameter cylindrical floating structure, with slack or taut mooring (e.g., Glanville et al, 1991). This concept has recently gained increased interest within the offshore community. For example, Oryx has installed the first production spar (Neptune) in 1996, while Chevron is currently designing the first spar (Genesis) for both drilling and production. Concurrently, a particular spar buoy has been designated the "theme structure" of the NSF-sponsored Offshore Technology Research Center (OTRC), centered at Texas A&M University and at the University of Texas at Austin.

This study compares analytical predictions of spar surge motions with the results of model tests from the OTRC wave tank (OTRC, 1995). Comparisons are shown both for summary response statistics and for complete time histories. Consistent choices of damping and wave input are considered in some detail. Responses are filtered and compared for three distinct frequency ranges: a relatively

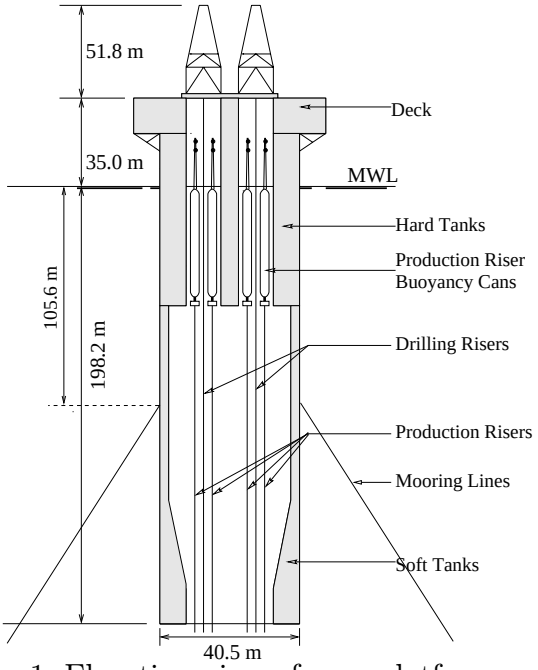

Figure 1: Elevation view of spar platform.

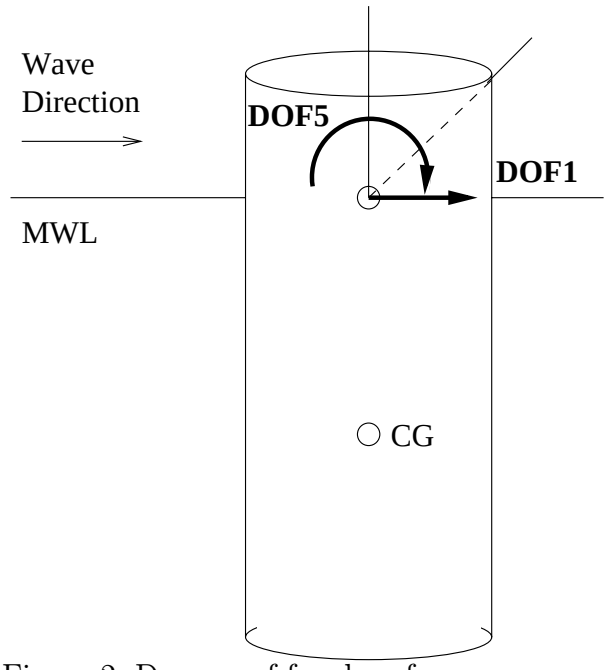

Figure 2: Degrees of freedom for spar.

high-frequency contribution due to first-order wave energy, a low-frequency contribution due to pitch, and a still lower frequency contribution due to surge. Model tests are studied for extreme (100-year) conditions in both the Gulf of Mexico and the North Sea.

Results from analytical models are shown here over a range of increasing modelling detail. The base case includes nonlinear diffraction forces and a linear, multi-degree-of-freedom structural model. Refinements on this include the addition of wave drift damping, and then of viscous forces as well. These successively more detailed models are generally found to yield improved agreement with model test results. The analytical predictions also show the ability to capture another notable feature of the spar model tests; namely, the apparent "mode-swapping," between the spar response in pitch and surge modes, during the hour-long tests.

Spar Buoy Characteristics

Figure 1 shows the prototype dimensions of the spar buoy under study. Note its relatively deep draft (H=198.2m), particularly with respect to its diameter (D=40.5m). For prediction purposes the spar buoy hull is assumed rigid, and its mooring lines are modelled as a set of massless, linear springs. To predict the spar's motions in the along-wave direction, we adopt a 2DOF model that includes the surge motion $x_1(t)$ and pitch rotation $x_5(t)$ at the mean water level* (Figure 2). At an elevation z above this level, the corresponding along-wave displacement of the rigid spar is predicted simply as $x_1(t) + z \cdot x_5(t)$. In particular, we apply this result here with z=54.8m, to compare with video-recorded surge motions at this elevation during the wave tests (OTRC, 1995).

Mode Shapes and Periods

Assuming small deformations, the 2×2 stiffness and mass matrices can be constructed from geometrical considerations (Jha, 1997). This mass matrix includes added mass terms, reflecting first-order

*Note that we retain the common convention that numbers surge and pitch DOFs as "1" and "5" respectively, although no other DOFs are included here.

wave radiation effects. The resulting mode shapes and natural frequencies are

$$f_1 = \frac{1}{330}\ [\text{Hz}],\ \boldsymbol{\phi}_1 = [1 \quad 0]^T; \qquad f_5 = \frac{1}{70}\ [\text{Hz}],\ \boldsymbol{\phi}_5 = [100 \quad 1]^T \tag{1}$$

These modal frequencies agree well with the natural periods, T_1=330s and T_5=67s, estimated from free-decay tests of the spar (OTRC, 1995). Note that this lower-frequency mode involves a pure translation, while the higher-frequency mode reflects a pure rotation about an axis located at depth 100m below the MWL. (Equivalently, Eq. 1 implies that a small rotation x_5 [rad] is accompanied by a translation of x_1=$100x_5$ [m] at the MWL.) These modes directly reflect the translational and rotational stiffnesses, respectively, of the spar's mooring system.

Qualitative Results and Consistent Damping Estimates

We consider here the spar model tests that reflect extreme, roughly 100-year wave conditions. We also focus on tests that apply wave loads only, neglecting other tests that include simultaneous current and/or wind loads. This leaves us with three model tests, each lasting 1 hour (all time and length units here reflect prototype scale). Two of the three are separate realizations of 100-year Gulf of Mexico seastates, while the third models 100-year North Sea conditions. We refer here to these seastates as "GOM1", "GOM2", and "NS". (In OTRC internal reporting, these tests are respectively denoted "aran3", "aran4", and "aran5". To date, only "aran3" has received systematic study by OTRC investigators; e.g., Ran et al, 1996, Weggel and Roesset, 1996).

Wave Measurements and Characteristics

A reference, "undisturbed" wave elevation history has been measured during the OTRC tests by a probe located 125m (prototype scale) from the spar, in a direction perpendicular to the wave direction. The spectra of these waves are found to be relatively well-fit by JONSWAP spectral shapes with γ=2; the significant wave height and peak period values are estimated as H_s=14.1m and T_p=14.1s for the Gulf of Mexico seastates, and H_s=14.8m and T_p=16.1s for the North Sea test (Jha, 1997). Note however that our response predictions use the observed wave histories from the tests, and not the simulated input from a theoretical wave spectral model.

Response Measurements and Characteristics

Figure 3 shows the power spectrum of the spar displacement, measured at height z=54.8m above MWL, during the GOM1 test. Note its two low-frequency modes, at around f_1=1/330 and f_5=1/70 Hz, reflecting motions induced by surge and pitch resonance. As Figure 3 shows, we use bandpass filters here to separate the observed surge component (0–.006 Hz), pitch component (.006–.03 Hz), and remaining wave frequency component (above .03 Hz). This gives rms response contributions of σ_{surge}=3.4m, σ_{pitch}=4.0m, and σ_{wave}=2.5m. Thus a linear force model, which predicts energy only at the wave frequencies, would capture only a small portion of the response rms. It would also completely fail to predict the mean response, here found to be 4.9m. The other tests offer similar results. This shows the need for models of nonlinear forces—diffraction, drag or both—to explain not only the mean offset but also the amplitude of slow-drift oscillations for the spar. The effects of both nonlinear diffraction and drag loads are considered below.

Figure 4 shows the corresponding time history of the response during the GOM1 test. Both the total response and its filtered components are shown. Consistent with its power spectrum in Figure 3, the response indeed displays three distinct time scales. What Figure 3 fails to reveal, however, is that the relative contribution of the different frequency components does not remain constant over time. For the GOM1 test, the observed response changes qualitatively at around t=1500s, when

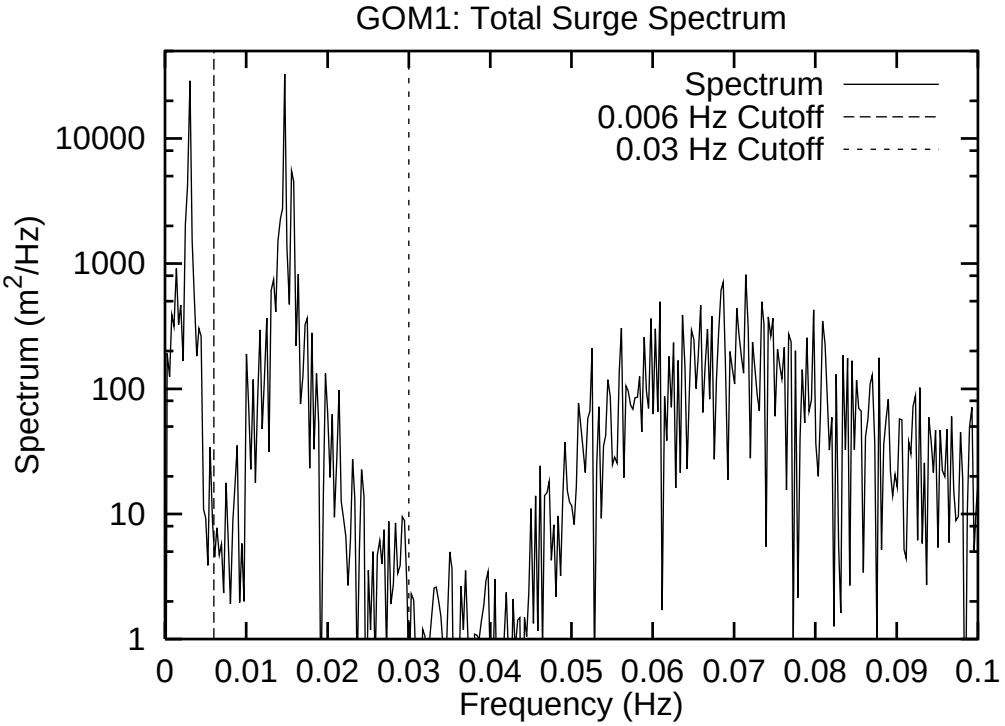

Figure 3: Spectrum of measured surge displacements at 54.8m elevation above MWL for GOM1 seastate

the surge component begins to contribute significantly. The other tests show somewhat similar shifts between the energy in surge and pitch modes—although this "mode swapping" is observed at different times, and for different durations, in different tests. The wave input histories show no such episodic nature. This reflects a further modelling challenge: can analytical models predict not only the correct average frequency content (e.g., the spectrum in Figure 3), but also time-domain behavior consistent with Figure 4? Clearly, this time-domain evolution of surge and pitch components depends directly on (1) their initial conditions at the beginning of the test recording and (2) the damping values assigned to these modes. We therefore discuss these issues, particularly damping estimation, in some detail.

Estimating Initial Conditions

In the experiments, spar motions were recorded after about 15 minutes (prototype scale), when the wave tank conditions were deemed to have achieved steady-state conditions. Thus, the assumption of at-rest initial conditions would corrupt our predictions, more so in the surge mode which contains relatively few cycles over the hour-long test. To avoid this, our predictions use initial conditions consistent with the tests; i.e., for each test we filter the observed motions to estimate surge and pitch components (e.g., Figure 4). The initial values/velocities of these components are then used to start our slow-drift motion predictions (Jha, 1997).

Estimating Surge and Pitch Damping

Because the tests include relatively few cycles of lightly damped motion, it is challenging to form precise damping estimates from them. We focus here on frequency-domain damping estimates, using response spectra from the various tests (e.g., Figure 3). One may, for example, select dampings

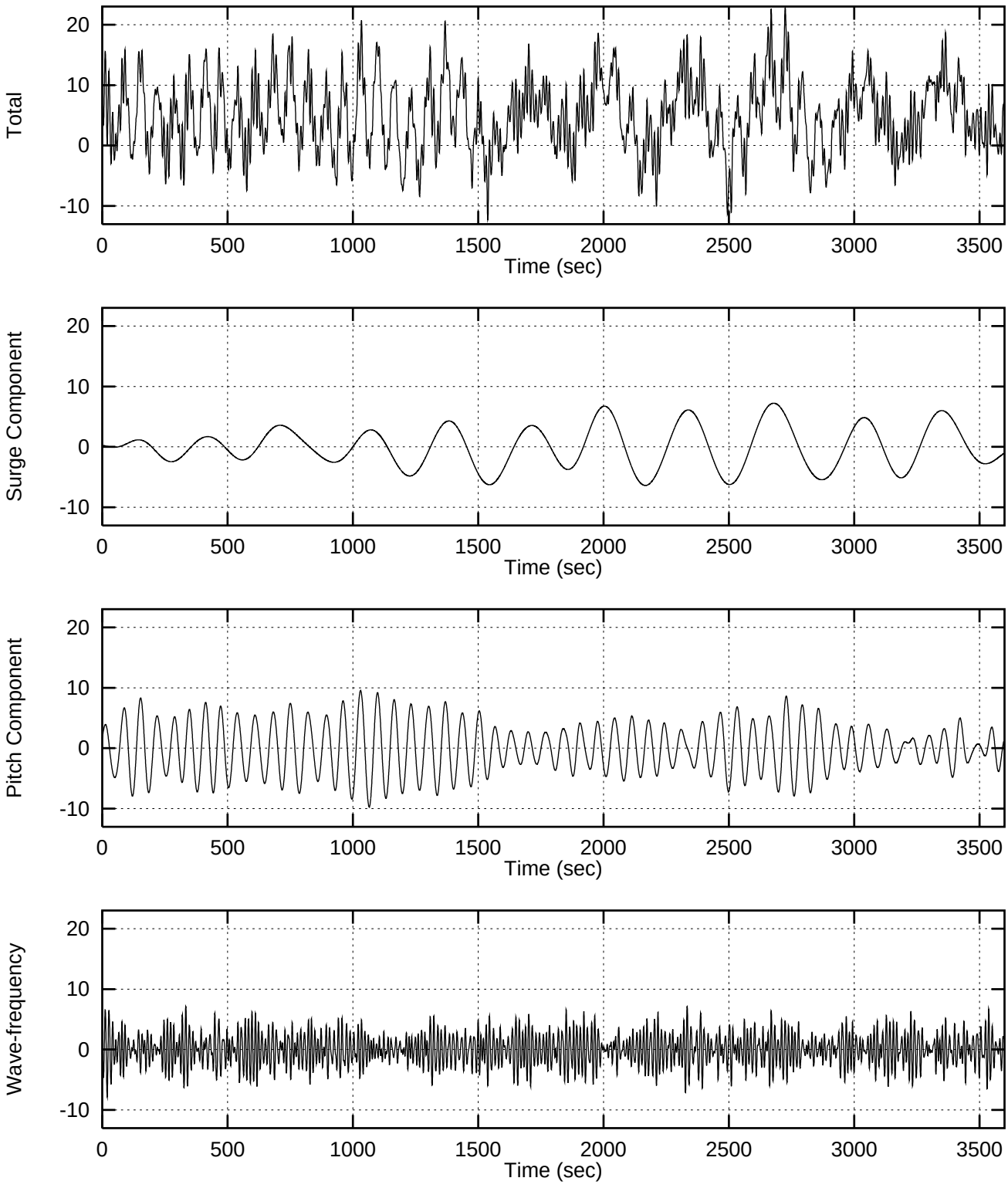

Figure 4: Total measured horizontal displacement and its filtered surge, pitch and wave-frequency components for GOM1 seastate

ζ_i so that our analytical model predicts the correct *area* under each of these observed spectral modes (i.e., the variances σ^2_{surge} and σ^2_{pitch}). A danger in this approach is that it may mask a force modelling error (e.g., Ude, 1994). For example, if predicted forces are overestimated we may overestimate damping in an effort to compensate. Thus, we instead seek damping values to preserve the observed spectral *shape*—the rms values σ_{surge} and σ_{pitch} are reserved to test the model's adequacy. One such measure of spectral shape is the half-power bandwidth, at which the response spectrum decays to half its peak value. By setting this bandwidth to its approximate value from theory—$f_{HP}=\pm\zeta_i f_i$ to either side of the natural frequency f_i—one can estimate the damping ζ_i from an observed power spectrum. For example, if the spar buoy has damping ζ_1=.05 at the surge frequency f_1=1/330, we find f_{HP}=1/6600 Hz. Unfortunately, from a T=1-hour history, our finest frequency resolution is df=1/T=1/3600 Hz—too coarse to resolve the half-power bandwidth, even if no frequency-averaging is applied to the observed spectrum.

We are therefore led to consider the average shape of the response spectrum across frequencies, as measured by the unitless bandwidth measure δ (Vanmarcke, 1972):

$$\delta = \sqrt{1 - \lambda_1^2/(\lambda_0\lambda_2)}\,; \quad \lambda_n = \int f^n S_x(f) df \tag{2}$$

Note that in general, any parameter of the form $\delta_n=[1-\lambda_n^2/(\lambda_0\lambda_{2n})]^{1/2}$ could be used to reflect bandwidth: $\delta_n \to 0$ as the bandwidth narrows. Perhaps the most widely used is δ_2, e.g, in modelling peaks of a Gaussian process. We use δ with n=1 here, as its lower spectral moments are less sensitive to high-frequency spectral content. We apply Eq. 2 twice, over the frequency ranges of surge (0–.006 Hz) and pitch (.006–.03 Hz) components, to find separate δ values that characterize their respective modal bandwidths.

For a 1DOF system under broad-band loads, δ can be related directly to the damping level (Vanmarcke, 1972, Ude and Winterstein, 1996). To form estimates consistent with our 2DOF model, however, we select damping ratios ζ_1 and ζ_5 so that our predicted response shows the same δ values, in both the surge and pitch frequency ranges, as found from the observed responses. This is an iterative process, which must be performed for each choice of (1) seastate and (2) predictive response model. We differentiate here between 2 seastates (GOM1 and GOM2 versus NS), and among 4 predictive models. These models are described below, together with the 2×4 values of modal dampings that result. In each case, a corresponding damping matrix $\boldsymbol{C}$ is inferred from the mass matrix and the matrix $\boldsymbol{\Phi}$ of modal shapes: $\boldsymbol{C}=\boldsymbol{M\Phi Q\Phi}^{-1}$ in terms of $\boldsymbol{Q}$=diag$(4\pi\zeta_i f_i)$.

Predictive Models of Forces and Damping

Our first, base-case model applies diffraction forces only (the "**DF**" model). Linear diffraction gives first-order transfer functions $F_1^{(1)}(\omega_k)$ and $F_5^{(1)}(\omega_k)$, the (complex) amplitude of surge force and pitch moment due to a unit-amplitude wave at frequency ω_k. A corresponding second-order diffraction analysis gives $F_1^{(2)}(\omega_k,\omega_j)$ and $F_5^{(2)}(\omega_k,\omega_j)$, the surge and pitch excitation amplitudes at the difference frequency $\omega_k-\omega_j$ due to pairs of incident waves at frequencies ω_k and ω_j (Kim and Yue, 1989; Kim and Yue, 1991). These subharmonic excitations drive the surge and pitch resonant motions, which dominate the spar response (e.g., Figure 3). Note that these diffraction forces assume as input not the undisturbed total wave elevation/potential but rather its first-order component. Here we use new methods (Winterstein and Jha, 1997) to identify the underlying first-order contribution to the observed undisturbed wave.

For this model, the damping matrix $\boldsymbol{C}$ gives the major source of damping. For example, Table 1 shows that this DF model requires the damping ratios ζ_1=4.5% and ζ_5=1.6% to match the spectral bandwidths estimated from the 2 GOM tests. In this (and other cases) the single NS test suggests rather lighter damping; indeed, an effectively zero value of pitch damping is not always able to give

Model	Description	GOM		NS	
		ζ_1	ζ_5	ζ_1	ζ_5
DF	Base-case model with diffraction forces	4.5	1.6	1.7	.001
DF/WDD	DF model plus wave-drift damping	3.3	0.6	.001	.001
DF/WDD/VF(u)	DF/WDD model plus viscous forces from undisturbed waves	4.0	0.5	2.5	.001
DF/WDD/VF(d)	DF/WDD model plus viscous forces from disturbed waves	6.5	.001	0.1	.001

Table 1: Description of 4 models, and consistent damping ratios ζ_1 and ζ_5 in surge and pitch.

as narrow a spectral bandwidth as observed. Note, however, that the NS test includes only a single hour, making narrow bandwidths more difficult to estimate than over the combined, two hours of GOM tests.

Our second model (**DF/WDD**) includes both diffraction forces and wave-drift damping. This damping force is proportional both to the structural velocity and to the square of the wave amplitude. The resulting nonlinear damping will tend to offset large slow drift forces, and perhaps reduce the extreme peaks of the surge response. We may expect that once wave drift damping is added, we require lower values of the additional modal damping ζ_i than in the DF model. Table 1 shows that this is indeed the case.

Finally, we also implement two models that include viscous drag forces as well as diffraction effects. These differ only in their choice of wave input: one uses the undisturbed waves, while the other uses the disturbed waves near the spar, inferred from its reported heave motions and the air-gap (structure-to-wave distance) measurements. Both models use the Morison's drag term with C_D=0.6, and Wheeler stretching (Wheeler, 1970) to integrate effects from the spar bottom to the free surface. They also both use the absolute fluid velocity; relative velocity effects are assumed reflected through damping terms.

Numerical Results

Wave-Frequency Response

We first compare the wave-frequency portions of the predicted and observed spar responses. These observed portions are found by applying a high-pass filter, with a low-frequency cutoff of .03 Hz., to the measured displacement histories. Figure 5 shows that these predictions fairly accurately predict not only the qualitative response behavior, but also its detailed cycle-by-cycle evolution in all three tests. This suggests that our models accurately reflect first-order wave forces, and the mass properties of the spar. (Because slow-drift forces and damping do not affect this wave-frequency response, all four of our models predict roughly the same histories in Figure 5. Thus, for clarity Figure 5 shows predictions only for the simplest (DF) model.)

Slow Drift Response

Figure 6 compares the predicted and observed moments of the slow-drift response. Results are shown for the rms values σ_1 and σ_5, corresponding to frequency ranges (0–.006 Hz) and (.006–.03 Hz), and for the total mean offset (which cannot be split directly into surge and pitch contributions).

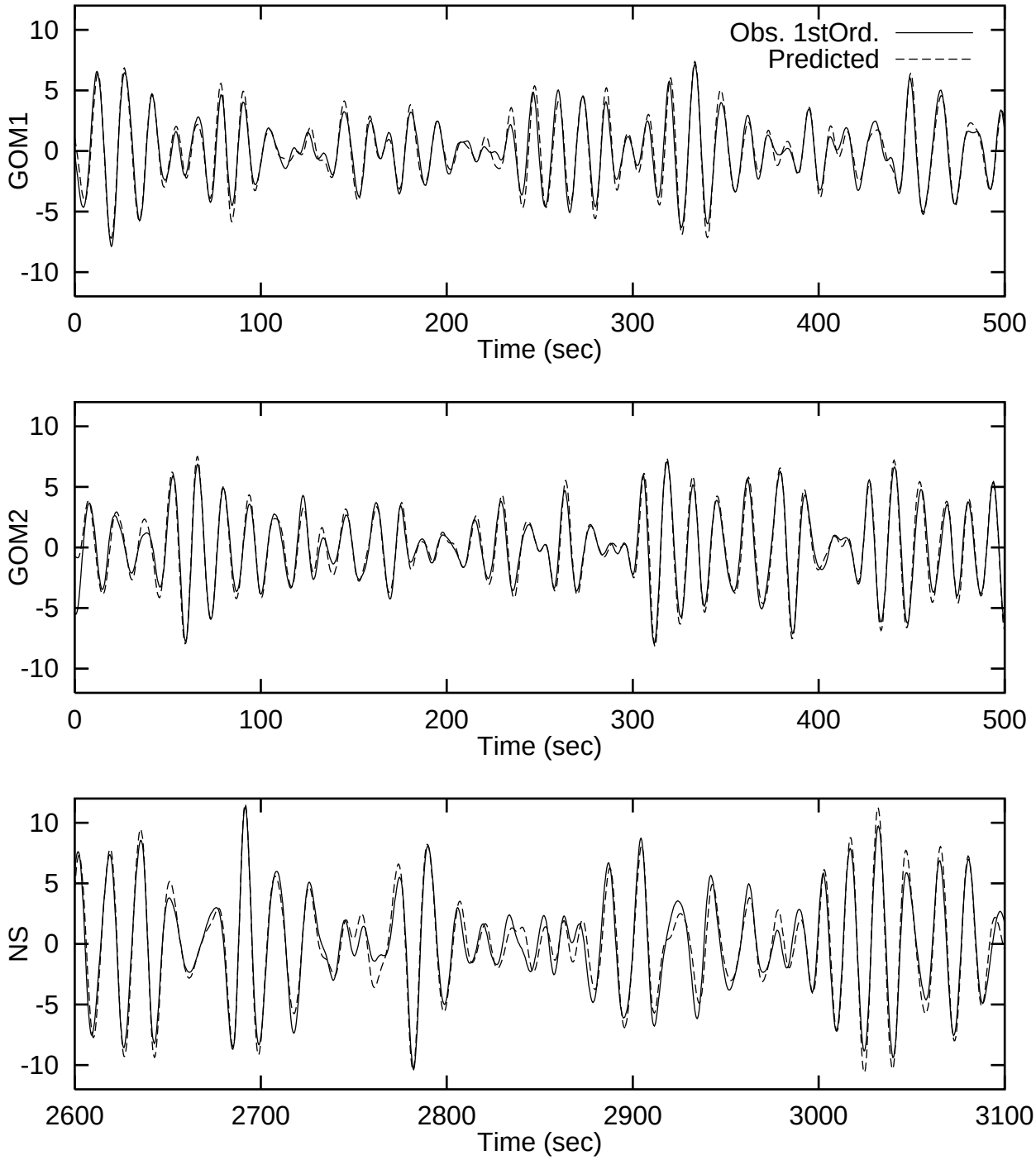

Figure 5: Predicted vs. observed first-order response histories for the three tests. For clarity we show only 500-second portions of each test, selected to include the absolute maximum observed response.

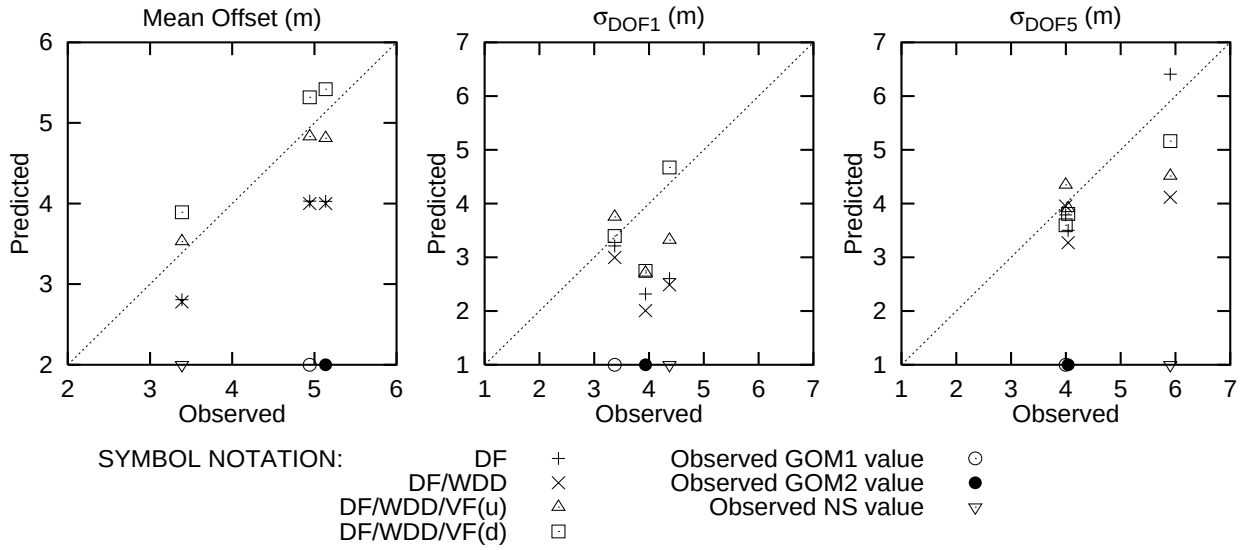

Figure 6: Predicted response mean and standard deviations vs measured results in the three tests. Standard deviations are shown for both surge and pitch frequency components.

In each case the predicted values from all 4 models are plotted against the observed value from that test. Because there are 3 tests, this results in 4×3=12 data points per plot. A 45-degree line implying perfect agreement is also shown.

Focusing first on the diffraction-only (DF) model, we find it underpredicts both the mean and rms in all but one of the 9 observed values. (We return below to the anomalous case, which involves the pitch rms σ_5 in the NS test.) Adding wave drift damping (DF/WDD) will not change the mean, and only weakly affects the rms predictions (again excluding the NS pitch case). This suggests the need for viscous forces, which contribute both an extra mean force (due to the asymmetric effect of wave stretching) and a slowly-varying drift force. As Figure 6 shows, the VF(u) and VF(d) models—which include viscous forces—generally give better predictions of both the mean and rms levels. Results with the disturbed wave (VF(d)) generally give slightly higher responses—both in mean and rms—than those using the undisturbed wave (VF(u)). Neither the VF(u) nor VF(d) model seems systematically closer to the observations; however, both appear superior to models that exclude viscous forces altogether.

Returning to the anamolous pitch response in the NS test, note from Table 1 that our damping calibration effectively fails in this case. Although each of the 4 models was assigned only minimal pitch damping (ζ_5=.001), all of these predict wider spectral bandwidths than that observed in the NS test. Thus the predictive models here are not "damping–tuned" to the tests as in the other cases—and the pattern of the 4 model predictions for σ_5 in the NS case is somewhat arbitrary. As to why the bandwidth mismatch may occur, recall the increased effect of limited data in the NS case: here the bandwidth estimation uses only the 1 hour test, as opposed to the 2 pooled hours used to form the predictive model for both GOM seastates.

Total Response Histories

Finally, we compare the observed and predicted 1-hour histories of the total spar displacement. Figures 7–9 show these histories for the 3 1-hour tests. All figures show the observed displacement history at the top, while 3 of the 4 corresponding predictions are shown beneath (the DF/WDD

model is omitted for clarity). Recall that our particular interest lies in predicting not only overall response statistics, but also the response evolution and potential mode-swapping (e.g., Figure 4 for the GOM1 case). Figure 7 repeats that case, and it is notable that all 3 predicted responses show a similar trend, toward greater surge response, in the second half of the GOM1 test. Note also that for extreme response events (e.g., observed response above 20m), all of the predictions show fairly good agreement. The greatest deviations, between the test and predictions, seem to occur over periods of relatively low response amplitude (e.g., times t=0–1000s, 1500–2300s).

Figure 8 shows similar tendencies for the GOM2 test. Again there is good qualitative agreement: both the tests and the predictions show a period of relatively little surge (at around t=700–2000s), followed by a marked surge increase through the rest of the hour. Large observed responses tend to coincide with high predicted values. The magnitude of these large responses is not as well predicted, however; predictions generally underestimate the response in the critical high-surge portion (t=2300–3600s). In contrast, the same predictions often overestimate response in the earlier, low-surge segment (t=700–2000s). (This potential for mode swapping and compensating errors suggests the need here to compare observations and predictions through time history behavior, not merely through summary statistics in the time or frequency domain.)

Finally, Figure 9 shows NS test results. Again there is a transition, near the end of the test, which produces the largest amplitude responses (indeed, the largest offsets among the 3 tests). It is caused here, however, by an increase in the pitch as well as the surge component. Note that despite the potential damping mismatch in this case, the models follow this critical portion of high-amplitude pitch fairly well (from about t=2700s on). As in the GOM1 case, greater deviations between models and observations occur at earlier portions of the history, involving lower amplitude responses.

Comparing Responses to Simulated and Observed Waves

The foregoing results show how well various models can predict the spar response in the OTRC tests, based on the corresponding observed wave input. Finally, we study briefly an associated question: are the observed response properties, such as mode swapping, also consistent with the response of the spar to idealized, Gaussian simulations of (first-order) random waves? If not, these observed properties may perhaps reflect special aspects of the wave input in the wave tank; e.g., the effect of its finite dimensions.

As earlier noted, both surge and pitch rms components of the observed spar motions vary notably over periods of roughly 20–30 minutes. We quantify this rms variation by (1) splitting the response into 20-minute segments; (2) calculating the rms values, $\sigma_1 ... \sigma_n$, in each of the n segments; and (3) forming the sample mean $\overline{\sigma}=\sum_i \sigma_i/n$ and variance $s_\sigma^2=\sum_i(\sigma_i-\overline{\sigma})^2/(n-1)$. We focus here on the two GOM tests, yielding 2 hours and hence n=6 20-minute segments with associated rms values $\sigma_1 ... \sigma_6$. The resulting s_σ values are found to be

$$s_\sigma = 1.22\text{m (surge)}\,; \quad s_\sigma = 0.50\text{m (pitch)} \tag{3}$$

For comparison we simulate† multiple 2-hour spar histories, and process each as we did the 2-hour test to find a corresponding s_σ estimate. These s_σ estimates from our simulations yield the following

†These simulations use the DF/WDD/VF(u) model, and first-order Gaussian waves are simulated from a JONSWAP spectrum with H_s=14m, T_p=14s, and γ=2. The diffraction analysis internally applies second-order corrections to the (assumed) first-order wave input; hence the Gaussian model is consistent here. Drag forces for this model use the total undisturbed wave; for simplicity we use the Gaussian waves here as well. Alternatively, one may add second-order wave contributions to better approximate the total undisturbed wave.

mean $E[s_\sigma]$ and standard deviation $D[s_\sigma]$:

$$E[s_\sigma] = 1.26\text{m (surge)}\,; \quad E[s_\sigma] = 0.95\text{m (pitch)} \tag{4}$$

$$D[s_\sigma] = 0.47\text{m (surge)}\,; \quad D[s_\sigma] = 0.45\text{m (pitch)} \tag{5}$$

Thus, while the observed modal rms values may seem highly variable, our simulations show similar or *still greater* variability (especially in pitch). Note also that the $D(.)$ values here reflect variability in s_σ estimates from different T=2 hour segments. (If T increases, $D(.)$ should decay like $T^{-1/2}$.) Because Eq. 3 uses 1 T=2 hour segment, these $D(.)$ values suggest the following mean $\pm$1-sigma intervals on the test estimates: s_σ=1.22 ± 0.47 in surge and s_σ=0.50 ± 0.45 in pitch. As even these relatively narrow, 1-sigma confidence intervals include the average simulation results (Eq. 4), it is difficult to find statistically significant differences between the tests and the simulations.

Conclusions

Four models have been established to predict the along-wave motions of a spar buoy in random seas. These have been implemented and compared with wave tank measurements of the spar displacement, at a reference elevation z=54.8m above the mean water level. Results are shown across 3 1-hour tests of 100-year extreme wave conditions. Specific methods and results include the following:

- In all of the tests, the main rms contribution comes from the resonant response in surge and pitch modes, at periods of roughly 330s and 70s respectively (e.g., Figure 3). This shows the need for models of nonlinear forces—diffraction, drag or both—to explain not only the mean offset but also the amplitude of slow-drift oscillations of the spar.

- The significant low-frequency resonant response also implies the need for accurate estimates of damping, in both the surge and pitch modes of the spar. We show how these modal dampings can be estimated from response spectral moments. The resulting dampings are "consistent" with the other features of the model; for example, the explicit addition of wave drift damping (WDD) is accompanied by lower levels of the remaining damping in the model (Table 1).

- The wave-frequency response has been found to be fairly well predicted across all 3 tests (Figure 5). This reflects the modelling adequacy of linear diffraction forces and the spar's mass properties. Regarding slow-drift response, models that include only diffraction forces generally underestimate both the mean and rms response levels (Figure 6). To address this, we introduce additional models that include viscous forces, based on either the undisturbed (far-field) wave or the actual disturbed wave in the presence of the spar. While it is difficult to conclude which of these is generally more accurate, both appear superior to models that exclude viscous forces altogether.

- The observed responses display considerable "mode-swapping" between surge and pitch modes (e.g., Figure 4). Figures 7–9 show that our predictive models, which use the observed wave and its underlying first-order components, can produce qualitatively similar behavior. They generally follow the observed trend, in all three tests, toward larger amplitude responses near the end of the hour. This trend manifests itself in the Gulf of Mexico tests by a late increase in surge-induced response (Figures 7–8), and in the North Sea test by enhanced pitch response as well (Figure 9).

- While the modal rms values in the tests appear rather variable, long simulations with Gaussian (first-order) waves show similar or *still greater* variability (Eqs. 3–5). From the limited 2-hour duration of GOM tests, it is difficult to find statistically significant differences between these tests and the simulations.

Acknowledgements

Support for this work has been provided by the National Science Foundation, through a grant from its Offshore Technology Research Center. We gratefully acknowledge the OTRC for their ongoing technical and financial support.

References

Glanville, R.S., J.R. Pauling, J.E. Halkyard, and T.J. Lehtinen (1991). Analysis of the spar floating drilling production and storage. *Proc., Offshore Tech. Conf.,* Houston, Paper OTC–6701, 57–68.

Jha, A.K. (1997). *Nonlinear stochastic models for ocean wave loads and responses of offshore structures and vessels,* Ph.D. thesis, Civil Eng. Dept., Stanford University.

Kim, M.H. and D.K.P. Yue (1989). The complete second-order diffraction solution for an axisymmetric body. Part 1: Monochromatic incident waves. *Journal of Fluid Mech.,* **200**, 235–264.

OTRC, Vol. I. (1995). *Spar model test: joint industry project,* Final Report, Offshore Technology Research Center.

Ran, Z., M.H. Kim, J.M. Niedzwecki, and R.P. Johnson (1996). Responses of a spar platform in random waves and currents (experiment vs. theory). *Int. Journal of Offshore and Polar Eng.,* **6**(1), 27–34.

Ude, T.C. (1994). *Second-order load and response models for floating structures: probabilistic analysis and system identification,* Ph.D. thesis, Civil Eng. Dept., Stanford University.

Ude, T.C. and S.R. Winterstein (1996). Calibration of slow-drift motions using statistical moments of observed data. *Proc., 6th Int. Conf. Offshore & Polar Eng.,* Los Angeles.

Vanmarcke, E. (1972). Properties of spectral moments with applications to random vibration. *J. Engrg. Mech.,* ASCE, **98**, .

Weggel, D.C. and J.M. Roesset (1996). Second-order dynamic response of a large spar platform: numerical predictions versus experimental results. *Proc., 15th Int. Conf. Offshore Mech. & Arctic Eng.,* Florence.

Wheeler, J.D. (1970). Method for calculating forces produced by irregular waves. *Journal of Petroleum Tech.,*, 359–367.

Winterstein, S.R. and A.K. Jha (1997). Random nonlinear ocean waves: a method to identify first- and second-order effects. *J. Engrg. Mech.,* ASCE, Submitted for possible publication.

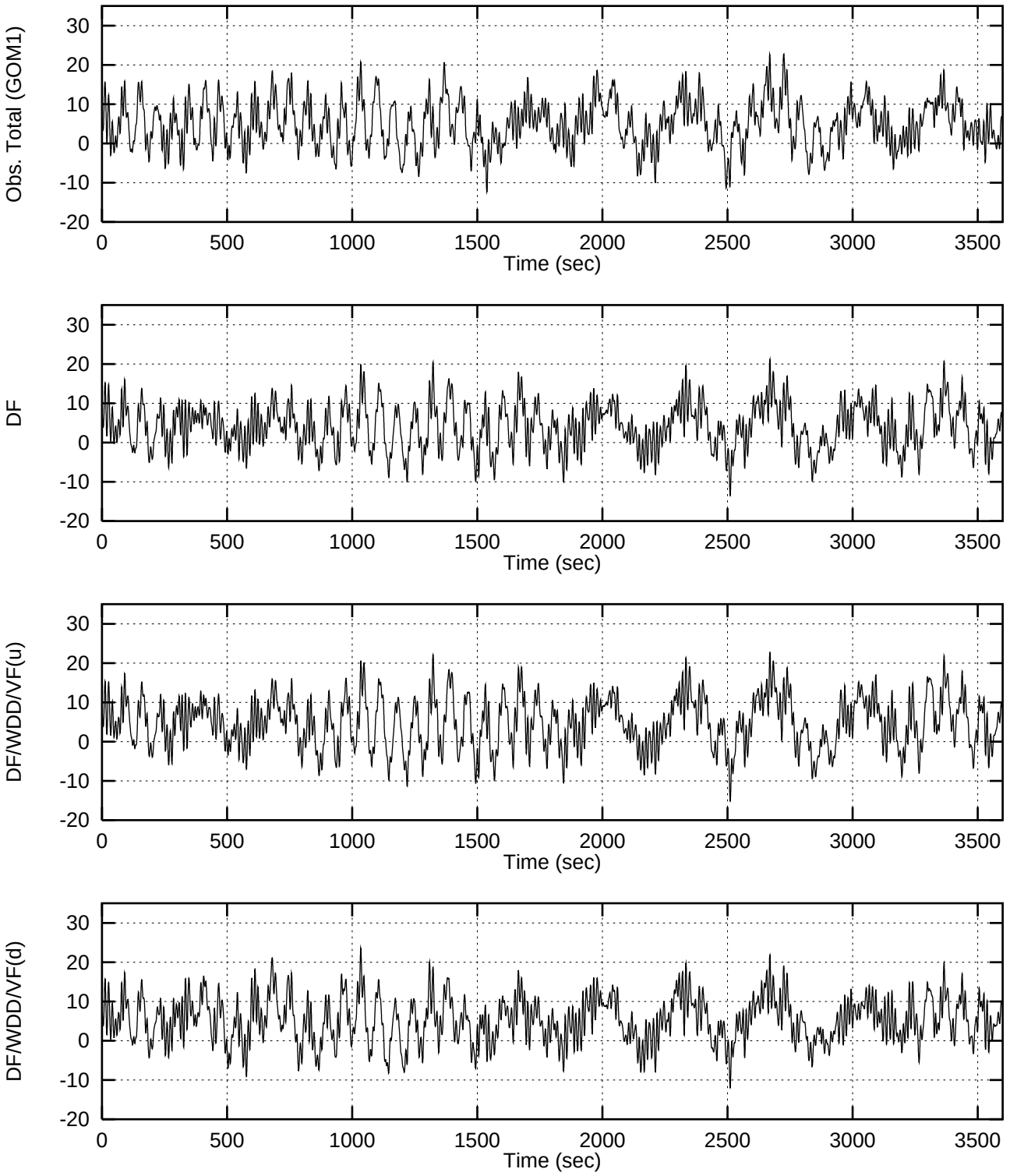

Figure 7: Combined (total) surge response time history for GOM1: prediction vs. measurement.

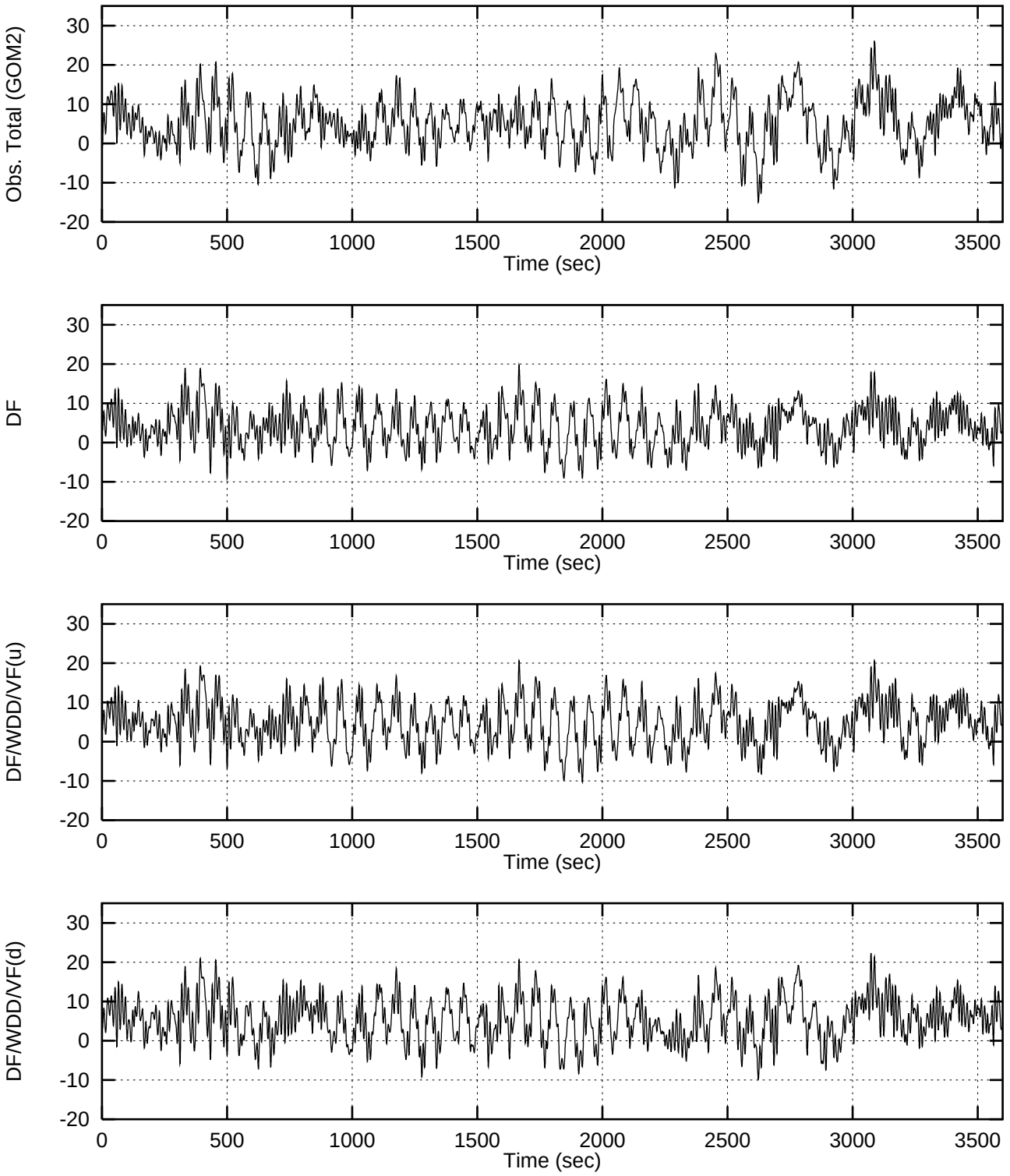

Figure 8: Combined (total) surge response time history for GOM2: prediction vs. measurement.

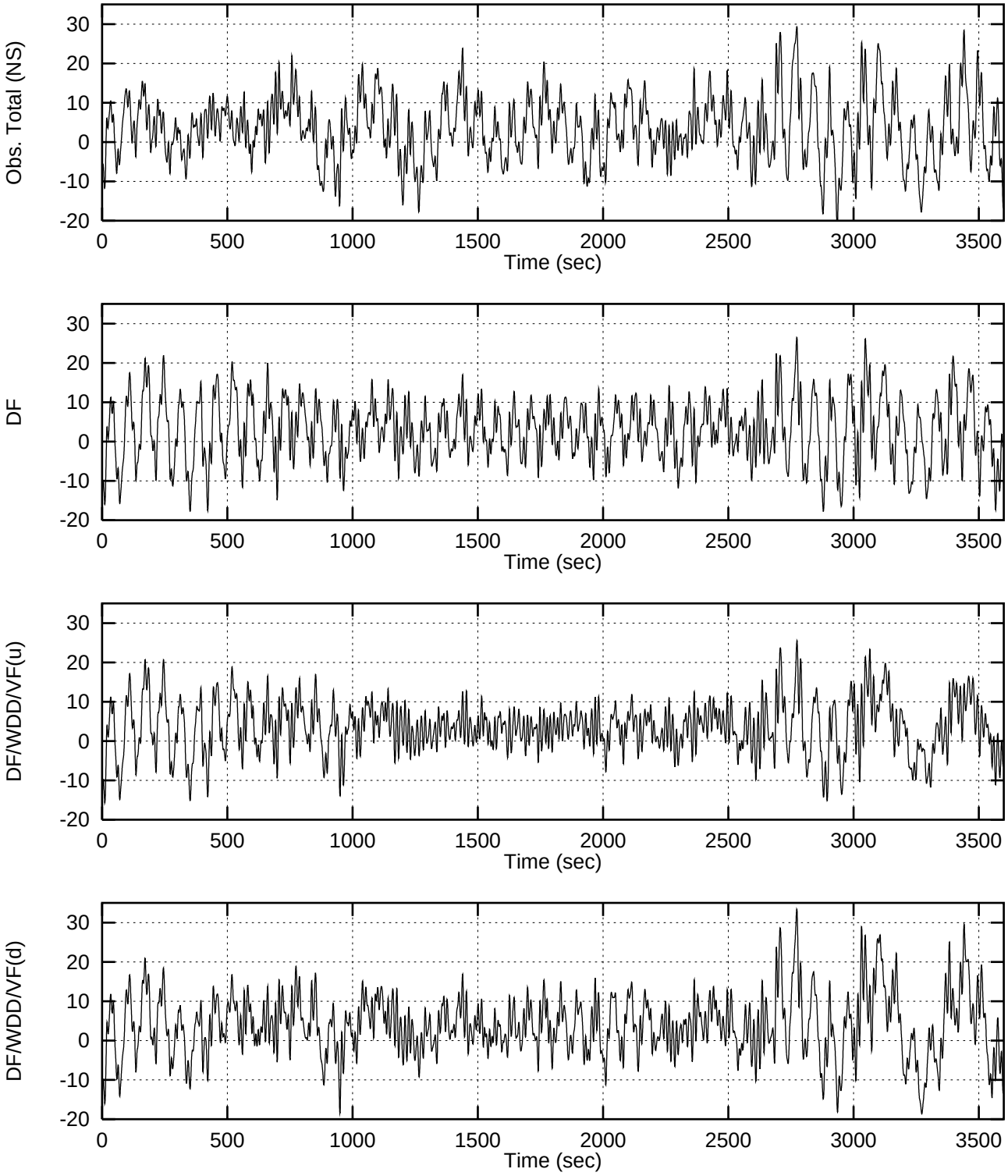

Figure 9: Combined (total) surge response time history for NS: prediction vs. measurement.